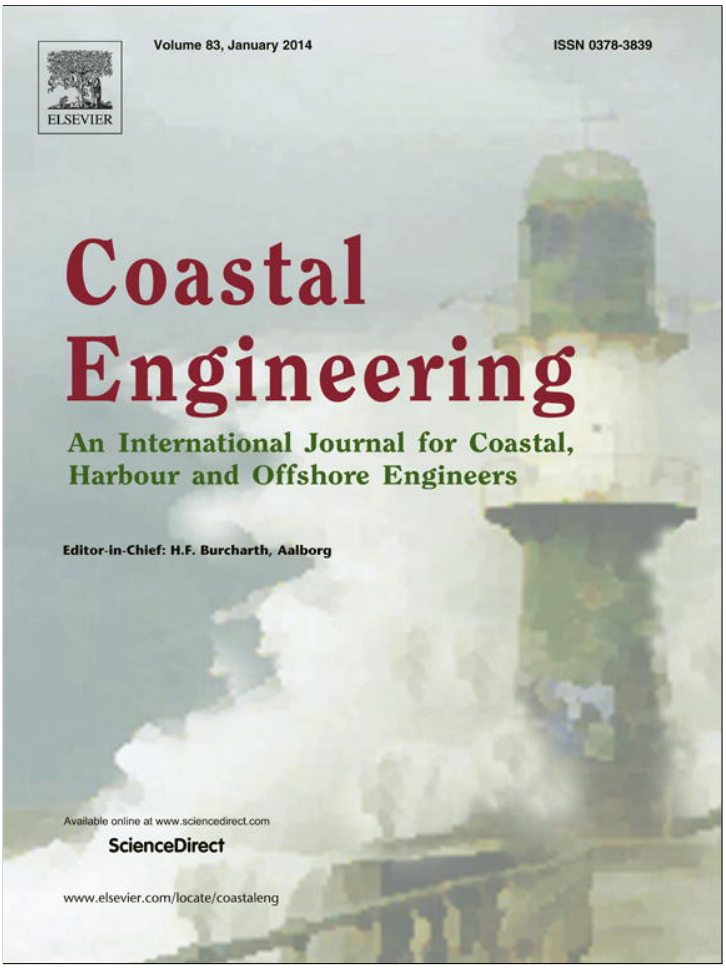

Coastal Engineering 83 (2014) 82–92

Contents lists available at ScienceDirect

Coastal Engineering

journal homepage: www.elsevier.com/locate/coastaleng

Wave attenuation by flexible, idealized salt marsh vegetation

M.E. Anderson *, J.M. Smith

Coastal and Hydraulics Laboratory, US Army Engineer Research and Development Center, Vicksburg, MS, USA

ARTICLE INFO

Article history:
Received 7 June 2013
Received in revised form 30 September 2013
Accepted 4 October 2013
Available online 30 October 2013

Keywords:
Vegetation damping
Wave dissipation
Wetlands
Spartina alterniflora
Drag coefficient
Equilibrium range

ABSTRACT

Wave attenuation by vegetation is a highly dynamic process and its quantification is important for understanding shore protection potential and modeling coastal hydrodynamics. Data documenting the interactions of *Spartina alterniflora*, represented by polyolefin tubing, and single- and double-peaked irregular waves were collected in a large-scale laboratory flume. The laboratory provided a controlled environment to evaluate wave attenuation, including the parameters of stem density, submergence, wave height, and peak period. Wave attenuation appeared to be most dependent on stem density and the ratio of stem length to water depth. Wave attention increased slightly with wave height while no clear trend with respect to wave period was seen. Treating double-peaked spectra as superimposed wave systems revealed a preferential dissipation of the higher-frequency wave system relative to the lower-frequency wave system under emergent conditions. Wave energy loss occurred at all frequencies of both spectral types, with dissipation increasing with frequency above the spectral peak. Parameterizing the spectral equilibrium range as a function of frequency showed a steepening of the spectral tail compared to the −4 power law under emergent conditions. An empirical relationship defining the bulk drag coefficient for *S. alterniflora* as a function of the stem Reynolds number is found to serve as a first estimate for engineering applications.

Published by Elsevier B.V.

1. Introduction

Coastal marshes serve as the interface between dry land and oceans throughout the world and are known to affect the local hydrodynamic climate (Koch et al., 2006). The aquatic vegetation comprising these systems is shown to drive the flow structure of unidirectional flows by controlling turbulence intensity, mass transport, and the development of mixing layers (Leonard and Luther, 1995; Nepf, 2012; Neumeier and Ciavola, 2004). With infrastructure and population ever-increasing along the coasts, the potential of coastal vegetation to mitigate storm damage and act as a non-intrusive buffer or "bioshield" is of recent increased interest (Feagin et al., 2009). Unfortunately, the contribution of vegetation to storm protection is largely unknown as rigorous experiments investigating the phenomena in the field are limited due to the unpredictable nature of storm development and the difficulty in deploying, maintaining, and retrieving instrumentation during these high-energy events; the only studies known to be conducted during tropical events were by Krauss et al. (2009), Smith et al. (2010), and Jadhav et al. (2013). Nevertheless, the need to quantify the impact of coastal vegetation on nearshore hydrodynamics has fueled research investigating the interactions of propagating water waves with vegetation. The majority of these studies have focused on bulk dynamics, such as the degree of wave height attenuation, with little discussion of the evolution of the wave energy spectra.

Coastal vegetation has shown to efficiently dissipate wave energy in low-energy environments. Field measurements documenting wave dissipation include intertidal zones in England, coastal mangrove ecosystems in Asia, salt marshes in the United States, and other studies. Table 1 summarizes the location and dominant plant species of known field studies documenting wave attenuation through vegetation. The earlier studies conducted by Wayne (1976) and Knutson et al. (1982) quantified wave dissipation only within the vegetation. Knutson et al. (1982) reported an average wave height reduction of 94% over 30 m, with 40% of the wave height dissipated within the first 2.5 m. Later studies compare colonized and bare areas to illustrate the capability of vegetation to modify the wave environment. Möller and Spencer (2002) measured considerably greater wave dissipation over inhomogeneous salt marshes than mudflats at two salt marsh–mudflat transition sites. An extensive yearlong study by Cooper (2005) found wave attenuation to be at least two times greater through salt marshes than mudflats, with the magnitude of attenuation differing between three transects. Wave attenuation in a coastal mangrove system was shown to be 5–7.5 times greater than bottom friction alone (Quartel et al., 2007). Since wave attenuation is a function of the coupled plant structure and nearshore hydrodynamics, this variability in wave attenuation is not surprising, and universally describing wave attenuation through vegetation is difficult (Méndez and Losada, 2004).

The interactions of waves with vegetation have also been studied in the laboratory, providing a controlled environment to evaluate wave attenuation with respect to individual plant and hydrodynamic

* Corresponding author at: Coastal and Hydraulics Laboratory, 3909 Halls Ferry Road, Vicksburg, MS 39180, USA. Tel.: +1 6016342074.
E-mail addresses: Mary.Anderson@usace.army.mil (M.E. Anderson), Jane.M.Smith@usace.army.mil (J.M. Smith).

0378-3839/$ – see front matter. Published by Elsevier B.V.
http://dx.doi.org/10.1016/j.coastaleng.2013.10.004

Table 1
Wave attenuation through vegetation field studies.

Study	Study site	Dominant plant species
Bradley and Houser (2009)	Florida	*Thalassia testudinum*
Cooper (2005)	UK	*Puccinellia maritima*, *Atriplex portulacoides*, *Salicorinia europaea*, *Spartina maritima*, *S. alterniflora*
Jadhav et al. (2013)	Lousiana	*S. alterniflora*
Knutson et al. (1982)	Virginia	*S. alterniflora*
Mazda et al. (2006)	Vietnam	*Sonneratia* sp.
Möller et al. (1999)	UK	Inhomogenous salt marsh
Möller and Spencer (2002)	UK	Inhomogenous salt marsh
Möller (2006)	UK	Inhomogenous salt marsh
Mork (1996)	Norway	*Laminaria hyperborea*
Paul and Amos (2011)	UK	*Zostera noltii*
Quartel et al. (2007)	Vietnam	*Kandelia candel*, *Sonneratia* sp., *Avicennia marina*
Vo-Luong and Massel (2008)	Vietnam	*Avicennia* sp., *Rhizophora* sp.
Wayne (1976)	Florida	*S. alterniflora*, *T. testudinum*
Ysebaert et al. (2011)	China	*Scirpus mariqueter*, *S. alterniflora*

parameters. The majority of laboratory work utilizes artificial plant mimics with limited studies focusing on real vegetation. Table 2 summarizes the element types as well as the vegetation of interest for known laboratory studies of wave attenuation through vegetation. Wave attenuation through four species of live vegetation varied between 20% and 76% over a 1-m test section, where the average reduction was about 40% for each species when leaf length was similar to water depth. Wave attenuation decreased as water depth increased or leaf length decreased, either singly or in combination (Fonseca and Cahalan, 1992). A parametric analysis of wave height, wave period, water depth, and plant density was conducted by Tschirky et al. (2000) using irregular waves. Wave attenuation increased with plant density and shallower water depths while neither incident wave height nor wave period demonstrated strong or conclusive trends. Augustin et al. (2009) investigated the dissipation of irregular waves over flexible and rigid vegetation to determine the effects of stem density for emergent and near-emergent conditions. Wave attenuation under emergent conditions was 50% to 200% greater per wavelength compared to near-emergent conditions, and wave attenuation increased with denser stem arrays. Little difference in attenuation was found between the flexible and rigid elements as the flexible elements never moved more than 20° from vertical. Wave damping through a submerged artificial kelp meadow increased with stem density, shallower water depth, and longer waves (Koftis et al., 2013). Like the field studies, the lab results are highly variable as the vegetation mimics differ in structure and response to wave forcing. Although the results demonstrate the capacity of vegetation to dissipate waves, the relative contribution of each parameter with respect to wave attention requires further attention.

Table 2
Wave attenuation through vegetation laboratory studies.

Study	Element	Plant species
Augustin et al. (2009)	Wooden dowels and polyethylene foam tubing	*S. alterniflora*
Dubi and Tørum (1996)	Molded plastic	*L. hyperborea*
Fonseca and Cahalan (1992)	Live plants	*Halodule wrightii*, *Syringodium filiforme*, *T. testudinum*, *Zostera marina*
Koftis et al. (2013)	Polypropylene stripes	*Posidonia oceanica*
Lima et al. (2006)	Nylon rope	*Brachiaria subquadripara*
Løvås and Tørum (2000)	Molded plastic	*L. hyperborea*
Manca et al. (2012)	Polypropylene stripes	*P. oceanica*
Mei et al. (2011)	Perspex cylinders	Not specified
Sánchez-González et al. (2011)	Polyethylene and polypropylene	*P. oceanica*
Stratigaki et al. (2011)	Polypropylene stripes	*P. oceanica*
Tschirky et al. (2000)	Live plants	*Scirpus validus*
Wu et al. (2011)	Live plants	*S. alterniflora*, *Juncus roemerianus*

More recent field studies have focused on the spectral dissipation of wave energy by vegetation. Lowe et al. (2007) performed experiments with submerged rigid cylinders and linked the large-scale dissipation of wave energy to the attenuation of in-canopy flow. The results showed frequency-dependent wave attenuation from the enhanced in-canopy flow generated by higher frequency wave components. Bradley and Houser (2009) studied the relative motion of flexible vegetation with implications to wave attenuation. Like Lowe et al. (2007), Bradley and Houser (2009) found the wave energy at higher frequencies to attenuate more. However, the spectral dissipation was attributed to relative seagrass motion as the in-canopy flow was assumed weak under low-energy conditions and further analysis showed the seagrass moving out of phase with the (higher) peak frequency but in phase with the (lower) secondary frequency. The greatest magnitude energy dissipation for bimodal spectra collected during Tropical Storm Lee was observed near the spectral peaks (wind sea component). The higher frequency wind sea (0.16–0.32 Hz) largely dissipated within the leading vegetation reach while the low-frequency swell (<0.16 Hz) propagated to the subsequent reach with little attenuation (Jadhav et al., 2013).

The quantification of wave dissipation by vegetation is needed for accurately modeling coastal hydrodynamics and has led to an increasing demand for models that capture wave transformation over vegetation fields. Standard practice in these models, an example being the STeady-state spectral WAVE model (STWAVE), is to account for energy dissipation using a bottom friction term, and several studies have derived friction factors to represent vegetation (Augustin et al., 2009; Camfield, 1977; Manca et al., 2012; Möller et al., 1999; Smith, 2007). However, bottom friction does not realistically describe the interactions of vegetation and waves as vegetation impedes flow throughout the water column rather than just along the sea bottom. To meet this need, several formulations estimating the horizontal wave-induced drag forces of a stem array using a bulk drag coefficient C_D have been derived. Early formulations focused on monochromatic waves and approximated vegetation as an array of rigid, vertical cylinders (Dalrymple et al., 1984; Kobayashi et al., 1993). Models accounting for plant motion were later proposed by Asano et al. (1992) and Méndez et al. (1999). Méndez and Losada (2004) expanded upon Dalrymple et al. (1984) to estimate random wave transformations over mildly sloped vegetation fields under breaking and nonbreaking conditions by assuming a Rayleigh distribution. Chen and Zhao (2012) critically examined models based on the Rayleigh distribution and proposed two new models for random wave attenuation over vegetation that were not limited to narrow-banded spectra. Calibrating these models to measurements is crucial as C_D is an empirical coefficient and accounts for our ignorance of the responses of different plant species to wave forcing (i.e., swaying).

The present study investigates irregular wave dissipation by arrays of idealized, flexible salt marsh vegetation (modeled after *Spartina alterniflora*) using comprehensive laboratory data. *S. alterniflora* is native to the Gulf of Mexico and East Coast wetlands of the United States, where it is the dominant emergent seagrass in the frequently flooded low marsh habitat (USDA and NRCS, 2012). *S. alterniflora* is classified as an invasive species on the West Coast as it has demonstrated an ability to outcompete the native populations, such as *Spartina foliosa* in the San Francisco estuary (Callaway and Josselyn, 1992). The study first investigates the roles of stem density, submergence, incident wave height, and peak period with respect to wave attenuation. Further insight into the transformation of wave energy spectra is provided by

exploring the frequency-dependence of wave attenuation using double-peaked spectra and the evolution of the equilibrium range. Lastly, a first estimate for a bulk drag coefficient C_D applicable for *S. alterniflora* is proposed following the analysis of Méndez and Losada (2004).

2. Methodology

2.1. Physical model setup

The experiments were performed at the U.S. Army Engineer Research and Development Center in Vicksburg, Mississippi. The flume measures 63.4-m long, 1.5-m wide, and 1.5-m deep, and is equipped with a computer-controlled electro-hydraulic piston wave generator. The wave flume is approximately 0.45-m deeper at the wave generator. The deep section housing the wave paddle is 5.4-m long, followed by a 1:44 slope for 19.5 m that connects to a 12.2-m long, 1.5 m-deep flat testing area. Behind the flat is an 11.3 m-long, 1:20 concrete slope.

In order to shoal waves to the desired depth and elevate the vegetation field above the concrete flume floor, a 1:20 plywood slope measuring 6.1 m was installed 19.6 m from the wave paddle at rest. A 12.2-m long, 0.25-m high flat false bottom was constructed flush with the plywood slope. The 9.8-m long vegetation field started approximately 26.9 m from the wave paddle (1.2 m after the transition from the plywood slope to the false bottom). The 1.2-m bare sub-area before the vegetation allowed for wave stabilization following wave shoaling and verification of the target conditions. An identical sub-area was created behind the vegetation to connect the setup to and avoid sampling near the existing 1:20 sloping beach face. This 1:20 concrete slope shoreward of the vegetation was lined with 5.0-cm thick filtration media wave absorber to reduce wave reflection (Fig. 1).

2.2. Idealized vegetation

It is important to reproduce the physical properties of the live plant species as well as possible in order to realistically represent the flow resistance of the plant canopy. After subjecting a variety of common materials to wave forcing, cross linked polyolefin (XLPO) tubing was selected to construct the idealized vegetation as it fulfilled two basic requirements: it reproduced the swaying motion of seagrass and remained upright in shallow water to model emergent conditions. To simulate the basic morphology of *S. alterniflora*, 6.4 mm diameter tubing was selected based on reports of average stem diameters near this value (Feagin et al., 2011; Jadhav et al., 2013; Wu et al., 2011; Ysebaert et al., 2011). The tubing was cut into equal lengths (l_s) of 41.5 cm.

Rigidity is shown to be a key mechanical property influencing wave attenuation. An analytical model for the wave-forced movement of single-stem vegetation derived by Mullarney and Henderson (2010) predicted dissipation through flexible stems was about 30% of that for rigid stems. Considering several different locations along the Louisiana coast and varying times of the year, Chatagnier (2012) estimated the modulus of elasticity for *S. alterniflora* as $E_v = 159.8$ MPa using the method of Freeman et al. (2000). However, *S. alterniflora* sampled in Texas was reported to have $E_v = 1410 \pm 710$ MPa by Feagin et al. (2011). While both researchers use traditional beam theory to calculate E_v, the methodologies and location of samples were different. Non-uniformity of the plant stem, plant age and health, water content, season, and salinity are all naturally occurring factors that could affect E_v (Feagin et al., 2011; Pezeshki et al., 1993; Salpeter et al., 2012; Touchette et al., 2009). As XLPO does not conform to Hooke's law for elastic materials, the 2% secant modulus is used for comparative evaluations to E_v (ASTM Standard D5323, 2011). XLPO tubing has a density of 1350 kg/m^3 and a maximum secant modulus of 172.4 MPa, which is close to the value for *S. alterniflora* reported by Chatagnier (2012) (ASTM Standard D3149, 2006). Unfortunately, the values of E_v reported in the literature for *S. alterniflora* differ by an order of magnitude. It is important to establish consistent values of E_v for *S. alterniflora* to minimize the impact rigidity will have on the degree of wave attenuation.

In natural *S. alterniflora* beds, stem density (N) is highly variable, depending upon the depth, health, and age of the stand. Two spatial densities of $N = 200$ and 400 stems/m^2 were tested, which correspond to a grid spacing of 7.1 and 5.0 cm. This density range is representative of natural *S. alterniflora* meadows (Knutson et al., 1982). The higher density configuration was constructed by adding additional elements to the previous lower density array (Fig. 2). The tubing was secured onto 2.0-cm thick plywood sheets using construction adhesive and wood screws, and these plant units were then fixed firmly together in the flume and secured to the setup. The idealized $N = 400$ stems/m^2 meadow installed in the flume is shown in Fig. 3.

2.3. Test conditions and instrumentation

Twenty-one irregular wave conditions were generated for this study (Table 3). Because wave signals were repeated for different stem configurations, the average incident zero-moment wave height H_0 at the leading edge of the vegetation and its standard deviation are given. The maximum standard deviation was less than 2.0 mm, indicating that nearly the same wave conditions were used for each phase of the experiment. Water depth at the vegetation was varied to model emergent conditions ($l_s/h > 1.0$), near-emergent conditions ($l_s/h = 0.91$), and more submerged conditions ($l_s/h = 0.78$), where submergence is defined using the ratio of average stem length l_s to water depth h. Waves were generated for 480 s to ensure the measurement of at least 200 waves and each signal were repeated a minimum of three times to check precision. Data were collected for a total of 63 tests.

Fifteen single-peaked irregular wave conditions were generated using a TMA shallow-water wave spectrum with spectral peakedness $\gamma = 3.3$. Incident wave height and peak period were systematically varied to analyze the effect of each parameter on wave dissipation. Peak period T_p ranged from 1.25 to 2.25 s and average zero-moment incident wave height H_0 varied from 5.0 to 19.2 cm, thus for intermediate water depth $0.08 < h/L_p < 0.18$, where L_p is the wavelength at the spectral peak, and for relative wave height $0.11 < H_0/h < 0.42$. Six double-peaked spectra with peaks at 1.25 and 2.0 s were also investigated. The double-peak spectra were synthesized by linearly superimposing two wave spectra with $\gamma = 10.0$. The larger γ values produce narrower spectral peaks with distinct separation in frequency.

Water surface oscillations were measured with 13 single wire capacitance-type wave gauges (WG) sampling at 25 Hz. WGs 1–3 formed an offshore Goda array to calculate reflection and were located at x = 6.1, 6.4, and 7.0 m with x = 0 at the wave paddle at rest (positive

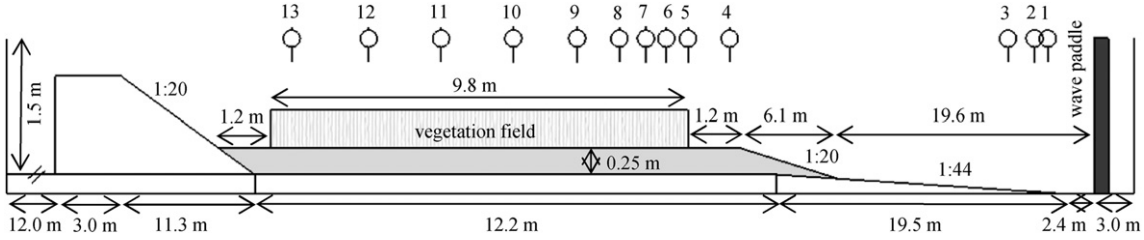

Fig. 1. Cross section of the flume and physical model setup (not drawn to scale). The white numbered circles are the locations of the wave gauges.

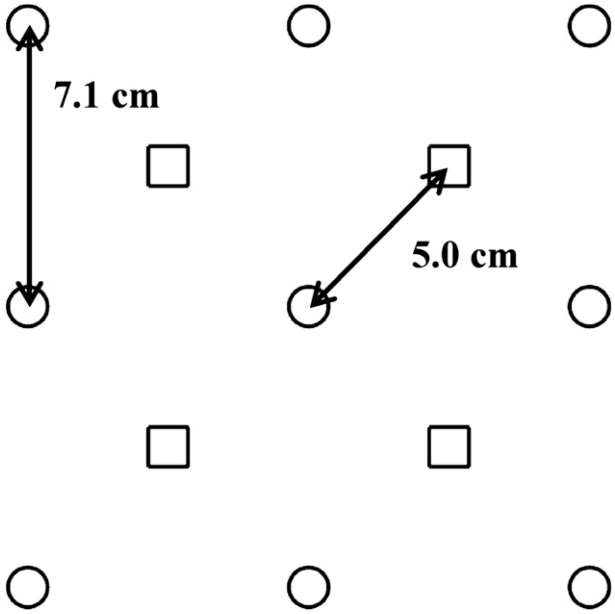

Fig. 2. Schematic of idealized vegetation stem configurations. The circles are $N = 200$ stems/m^2. The addition of a center stem, indicated by the square, increases the density to $N = 400$ stems/m^2.

Table 3
Incident single- and double-peaked irregular wave conditions measured at the beginning of the vegetation (WG 5).

Wave type	Depth h (cm)	Wave height H_0 (cm)	Peak period T_p (s)	Peak wavelength L_p (m)	l_s/h (−)	H_0/h (−)	h/L_p (−)
Single-peaked	53.3	11.1 ± 0.07	1.5	2.89	0.78	0.21	0.18
	53.3	11.0 ± 0.10	1.75	3.53	0.78	0.21	0.15
	53.3	11.2 ± 0.06	2.0	4.16	0.78	0.21	0.13
	45.7	8.1 ± 0.03	1.5	2.74	0.91	0.18	0.17
	45.7	10.9 ± 0.05	1.5	2.74	0.91	0.24	0.17
	45.7	13.9 ± 0.07	1.5	2.74	0.91	0.30	0.17
	45.7	5.0 ± 0.03	2.0	3.91	0.91	0.11	0.12
	45.7	10.7 ± 0.04	2.0	3.91	0.91	0.23	0.12
	45.7	15.3 ± 0.10	2.0	3.91	0.91	0.33	0.12
	45.7	19.2 ± 0.14	2.0	3.91	0.91	0.42	0.12
	30.5	11.3 ± 0.09	1.25	1.88	1.36	0.37	0.16
	30.5	11.0 ± 0.11	1.5	2.36	1.36	0.36	0.13
	30.5	11.2 ± 0.10	1.75	2.82	1.36	0.37	0.11
	30.5	11.1 ± 0.16	2.0	3.28	1.36	0.36	0.09
	30.5	11.2 ± 0.13	2.25	3.73	1.36	0.37	0.08
Double-peaked	53.3	13.7 ± 0.04	1.25/2.0	–	0.78	0.26	–
	53.3	10.9 ± 0.03	1.25/2.0	–	0.78	0.20	–
	45.7	13.6 ± 0.04	1.25/2.0	–	0.91	0.30	–
	45.7	10.7 ± 0.05	1.25/2.0	–	0.91	0.23	–
	30.5	13.0 ± 0.18	1.25/2.0	–	1.36	0.43	–
	30.5	10.7 ± 0.14	1.25/2.0	–	1.36	0.35	–

toward the shoreline). WGs 4–13 were installed along the center of the channel at x = 26.0, 26.9, 27.4, 27.9, 28.5, 29.5, 31.0, 32.7, 34.4, and 36.2 m, in that order (Fig. 1). WGs were calibrated daily to minimize calibration error and to ensure that wave heights were bounded by the calibrated range.

3. Wave height attenuation analysis

Reflection coefficients for the flume were estimated using a three-gauge separation technique based on the method of Goda and Suzuki (1976). The wave reflection analysis was performed using WGs 1–3, and reflection coefficient K_r varied from 5% to 12%. There was little change in K_r between the setup with and without vegetation. The mean reflection coefficients were 8.2%, 8.3%, and 8.7% for $N = 0$, 200, and 400 stems/m^2, respectively. As K_r remained relatively small, the effect of wave reflection on the results was considered negligible. Wave reflection from the absorber-covered back slope was not calculated.

The effects of stem density, submergence, incident wave height, and peak wave period on wave propagation were evaluated using measurements of wave height. The wave spectral density $S(f)$ at each gauge was extracted from the demeaned water surface elevation time series with a fast Fourier transformation. The data were broken into segments of 2048 points, and the spectra were smoothed by averaging five neighboring frequency bands. The resulting resolution bandwidth was 0.061 Hz, and spectral estimates had 60° of freedom. The local zero-moment wave height H was estimated from the wave spectra

Fig. 3. Installed idealized vegetation bed ($N = 400$ stems/m^2).

(with an upper frequency cutoff of 2 Hz) using the following relationship:

$$H = 4\sqrt{\sum_{j=1}^{n} S(f)_j \Delta f} \quad (1)$$

where n is the number of frequency components and Δf is the frequency resolution. The root-mean-square height H_{rms} was obtained directly from the demeaned time series record:

$$H_{rms} = \sqrt{\frac{1}{M}\sum_{j=1}^{M} H_j^2} \quad (2)$$

where H_j is the individual wave heights in a record containing M waves.

3.1. Wave height attenuation

Control tests served to measure the background attenuation losses due the bare plywood setup and the concrete/glass flume walls. The energy loss for waves propagating through the control and $N = 400$ stems/m^2 is shown in Fig. 4, where spectral transformations are presented for one wave condition ($l_s/h = 1.36$, $H_0/h = 0.37$, $h/L_p = 0.11$). Spectra are shown for WGs 1, 5, 7, 10, and 13, which are at $x = -20.8$, 0.0, 1.0, 4.1, and 9.3 m where x is the distance from the front edge of the vegetation. A greater loss of wave energy is observed at all frequency components for the vegetation compared to the control, with the most evident loss of wave energy observed at the peak frequency. Higher frequency harmonics, such those around 1.2 Hz, are generated as the waves propagate from the wave paddle (WG 1) to the setup (WG 5). These high-frequency variations persist in the control spectra, but are dissipated by the end of the vegetation field.

Wave attenuation was quantified using an exponential decay function of the form:

$$\frac{H}{H_0} = \exp(-k_i x) \quad (3)$$

where H is the local wave height, H_0 is the incident wave height (measured at the leading edge of the vegetation at WG 5), k_i is the wave decay coefficient, and x is the horizontal distance between the gauges (Kobayashi et al., 1993). The decay coefficient k_i was calculated by fitting the normalized zero-moment wave height H/H_0 to Eq. (3) using the Gauss–Newton method of solving nonlinear least-squares. The goodness of fit was indicated by the squared correlation coefficient R^2 where $R^2 = 1.0$ indicates a perfect fit.

The exponential decay assumption described the wave decay behavior of the single- and double-peaked spectra well, with two single-peaked wave conditions having a $R^2 < 0.80$ (0.67 and 0.79). These lower R^2 values are associated with the control. R^2 exceeded 0.95 and 0.98 for $N = 200$ and 400 stems/m^2, respectively, for all single-peaked wave conditions. For the double-peaked spectra, R^2 exceeded 0.90 for the control and 0.98 for $N = 200$ and 400 stems/m^2. Decay coefficient k_i ranged from 0.006 to 0.019 m^{-1} for the control and 0.020 to 0.121 m^{-1} for the vegetation.

3.2. Behavior of the wave decay coefficient

The exponential decay coefficient increased with stem density for all modeled single- and double-peaked wave conditions. The average k_i for $N = 400$ stems/m^2 was 0.07, nearly twice as large as $N = 200$ stems/m^2 (average $k_i = 0.04$) and almost seven times larger than the bare control (average $k_i = 0.01$).

3.2.1. Single-peaked spectra

The effect of submergence on wave attenuation is shown in the upper left panel of Fig. 5, where k_i is plotted for the same single-peaked wave condition ($H_0 = 11.0$ cm, $T_p = 1.5$ s) and the control, $N = 200$ and 400 stems/m^2. Although a submergence ratio (l_s/h) is spurious for the bare control setup, the influence of vegetation on wave decay is assessed through a comparison between the control and vegetation measurements under identical forcing, in this case the same water depth. The exponential decay coefficient k_i increased with greater l_s/h considering the same density, with the greatest amount of attenuation observed during emergent conditions. Moreover, the rate at which k_i changes with l_s/h is coupled to stem density. Assuming a linear regression model, the change in k_i with l_s/h for the control was very mild, approximately 0.01. This slight increase was likely due to the increased friction induced by the bare setup in shallower water. However, the gradient of k_i for the idealized vegetation was considerably larger than the control and increased with stem density from 0.08 for $N = 200$ stems/m^2 to 0.13 for $N = 400$ stems/m^2. This increase in the slope

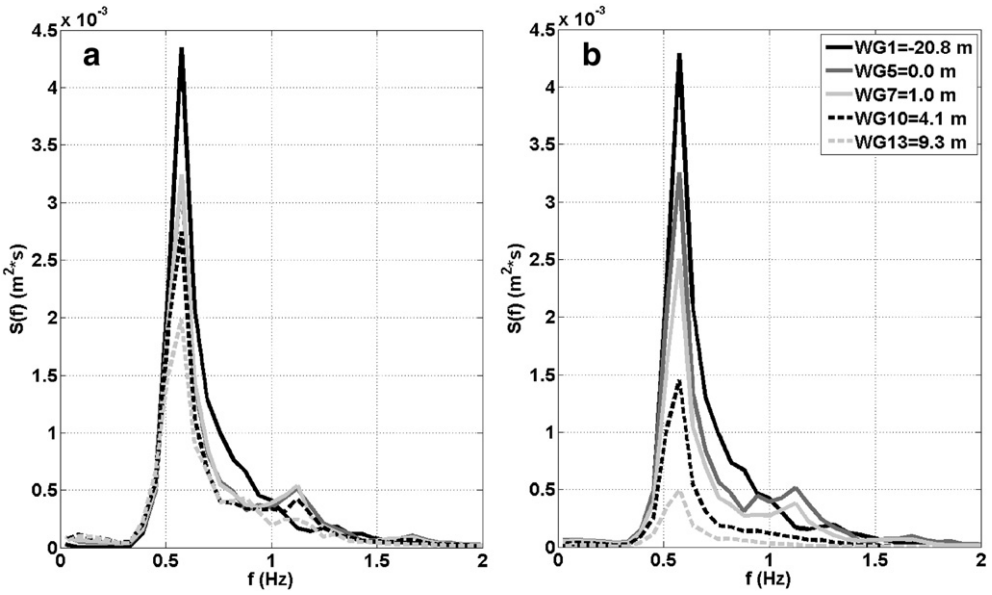

Fig. 4. Wave spectral transformation through (a) control and (b) $N = 400$ stems/m^2 for $l_s/h = 1.36$, $H_0/h = 0.37$, and $h/L_p = 0.11$.

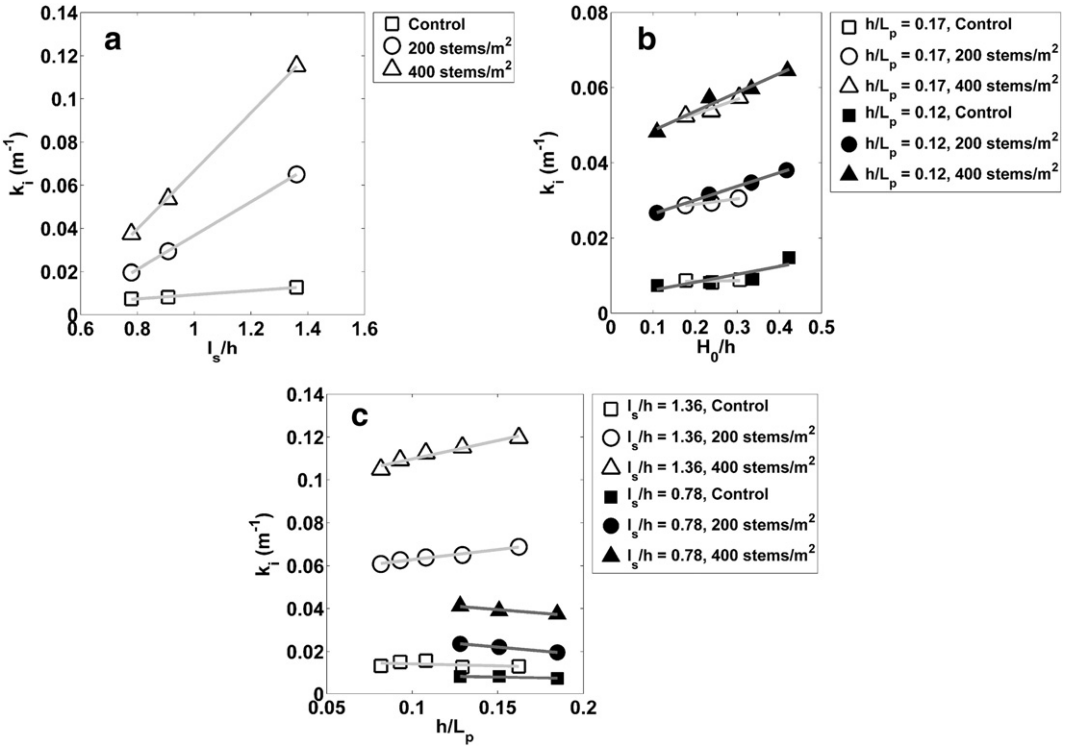

Fig. 5. Effect of (a) stem submergence ratio for $H_0 = 11.0$ cm, $T_p = 1.5$ s, (b) relative wave height for $l_s/h = 0.91$ (open symbols are $h/L_p = 0.17$ and closed symbols are $h/L_p = 0.12$), and (c) relative depth (open symbols are $l_s/h = 1.36$, $H_0 = 11.2$ cm and closed symbols are $l_s/h = 0.78$, $H_0 = 11.1$ cm) on decay coefficient k_i. The control case is represented by squares, $N = 200$ stems/m^2 by circles, and $N = 400$ stems/m^2 by triangles in each plot. Trend lines fit to each series are also shown.

of k_i suggests that stem density becomes more influential on wave decay with greater emergence.

The effect of the incident wave height on wave decay is shown in the upper right panel of Fig. 5 for all tested densities, including the control. Decay coefficient k_i increased with larger H_0/h for both periods tested ($h/L_p = 0.17$ and 0.12) considering the same density and submergence ($l_s/h = 0.91$). Although there was nearly no change in k_i with H_0/h for the $h/L_p = 0.17$ control (gradient of approximately 0.00), the slope increases to 0.01 for $N = 200$ stems/m^2 and to 0.04 for $N = 400$ stems/m^2. This trend was also seen for $h/L_p = 0.12$. The change of k_i with H_0/h was largest for $N = 400$ stems/m^2 (0.05), which was slightly greater compared to $N = 200$ stems/m^2 (0.04) and the control (0.02).

Wave attenuation as a function of peak period was explored using relative depth h/L_p. Waves are classified as deepwater when $h/L_p > 0.5$ and shallow-water when $h/L_p < 0.05$. The wave decay coefficient k_i slightly increased with h/L_p in the vegetation for the emergent condition $l_s/h = 1.36$, as seen in the bottom panel of Fig. 5. The slope of k_i for the control, N = 200 and 400 stems/m^2 for $l_s/h = 1.36$ was −0.02, 0.09, and 0.17, respectively. However, at the most submerged condition $l_s/h = 0.78$, k_i slightly decreased with larger h/L_p. Although k_i decreased more rapidly with h/L_p in the presence of vegetation compared to the control (−0.02), the rate of decrease was approximately similar for both $N = 200$ and 400 stems/m^2 (−0.07), unlike the other parameters. The reason for this conflicting trend in k_i is unclear. Unfortunately, the range of periods for this study was limited to the intermediate depth range and the influence of peak period on wave attenuation has been largely overlooked for emergent conditions. Additionally, studies focusing on submerged vegetation have been contradictory: Stratigaki et al. (2011) and Lowe et al. (2007) found that shorter-period waves were dissipated more effectively while Manca et al. (2012) and Cavallaro et al. (2010) observed an increase in wave attenuation with longer waves.

3.2.2. Double-peaked spectra

Previous studies of wave propagation through vegetation focused on field studies and single-peaked spectra, with the transformation of double-peaked spectra through vegetation largely unaddressed. In this study, double-peaked spectra were generated to investigate the dissipation of superimposed wave spectra by vegetation. Treating a double-peaked spectrum as the linear superposition of two wave systems, each spectrum was split into two frequency ranges by finding local minimum between the two peaks ($T = 1.25$ and 2.0 s). A decay coefficient k_i was calibrated for each of the resulting spectra.

The attenuation of the two frequency ranges was not uniform and depended on submergence and stem density. The decay coefficients are nearly identical for the separated wave systems under submerged conditions, but a larger k_i was calibrated for the higher-frequency spectra than the low-frequency spectra under emergent conditions for both the control and the vegetation (Fig. 6). However, dissipation of the higher-frequency system is enhanced for denser stem arrays. The difference in k_i between the two wave systems for $H_0/h = 0.35$ at $l_s/h = 1.36$ is 0.017, 0.035, and 0.044 m^{-1} for the control, $N = 200$ and 400 stems/m^2, respectively. This growing gap in k_i suggests that vegetation dissipates wave energy more efficiently among the higher frequency components of a double-peaked wave spectrum, particularly during emergent conditions, compared to the bare control. A similar trend in k_i was found for the other double-peaked spectra.

4. Spectral attenuation analysis

Previous studies of wave dissipation through vegetation have shown wave energy to be dissipated at different rates among the spectral components (Bradley and Houser, 2009; Jadhav et al., 2013; Koftis et al., 2013; Lowe et al., 2007). Assuming linear wave theory is valid, the change of wave energy ε at each jth component of the wave spectrum

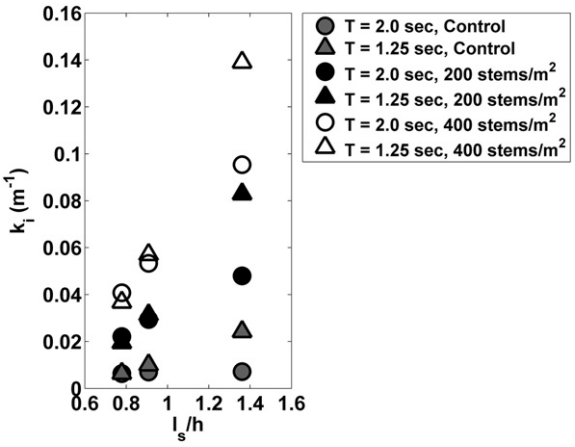

Fig. 6. Decay coefficient k_i for separated wave systems of double-peaked spectra versus submergence ratio for $H_0 = 10.7$ cm. The higher-frequency wave system is represented by triangles and the lower-frequency wave system is represented by circles. The color of the shape indicates density, where gray is the control, closed is $N = 200$ stems/m^2, and open is $N = 400$ stems/m^2.

as a function of the initial energy can be described by rearranging the conservation of energy flux equation:

$$\frac{\partial E_j}{E_j} = \frac{-S_{v,j}\partial x}{C_{g,j}E_j} = \varepsilon \tag{4}$$

where E is the wave energy density, C_g is the group velocity, and S_v is the time-averaged rate of energy dissipation induced by the vegetation per unit horizontal area. This form of the conservation of energy flux equation assumes that all other source or sink terms are negligible compared to vegetation-induced dissipation. The component wave energy density is given by:

$$E_j = \frac{1}{2}\rho g a_j^2 \tag{5}$$

where ρ is the water density, g is the gravitational constant, and a is the wave amplitude for each frequency, obtained from the wave spectral density:

$$a_j = \sqrt{2S(f)_j \Delta f}. \tag{6}$$

The energy dissipation with respect to frequency was calculated between three pairs of wave gauges (WG 5–WG 7, WG 5–WG 10, and WG 5–WG 13) within the vegetation.

Smoothed energy spectra and the change in energy between wave gauge pairs are shown in Fig. 7 for one single-peaked ($l_s/h = 1.36$, $H_0/h = 0.36$, $h/L_p = 0.09$, $N = 400$ stems/m^2) and double-peaked ($l_s/h = 1.36$, $H_0/h = 0.43$, $N = 400$ stems/m^2) wave condition. Wave energy dissipation is observed at all frequencies of the wave spectra for both spectra except around f = 1.5 Hz for reach WG 5–WG 7. This is likely due to the nonlinear transfer of energy to harmonic frequencies following wave shoaling, such as those at f = 1.0 and 1.5 Hz in the single-peaked spectra. The generation of harmonics for the double-peaked spectra is harder to identify. The percent decrease in energy for reach WG 5–WG 7 fluctuates considerably in both spectral types. However, the energy loss with respect to the initial energy generally increases with higher frequencies for both spectra in reach WG 5–WG 10. The secondary higher peak ($f = 0.8$ Hz) in the double-peaked spectra experiences a slightly greater relative loss than the dominant lower peak ($f = 0.5$ Hz). In reach WG 5–WG 13, the change in energy has stabilized compared to the shorter reaches, with the relative loss in energy for frequencies higher than the peak approaching 100%. This trend was also seen for the double-peaked spectra, where energy losses continuously increased with higher frequency relative to the initial energy. The more efficient dissipation of higher-frequency wave components are supported by field observations over seagrasses under low energy conditions (Bradley and Houser, 2009) and studies of in-canopy flow structure within submerged rigid canopies (Lowe et al., 2007). This frequency-dependent wave attenuation became less pronounced at smaller submergence ratios as less wave attenuation occurred.

5. Equilibrium range analysis for single-peaked spectra

Parameterization of the equilibrium range of deepwater and finite-depth wave frequency spectra has long been a topic of great interest, explored more recently by Resio et al. (2004) and Smith and Vincent (2003). Phillips (1958) characterized the equilibrium range based on an f^{-5} power law while recent studies have shown the spectral tail to

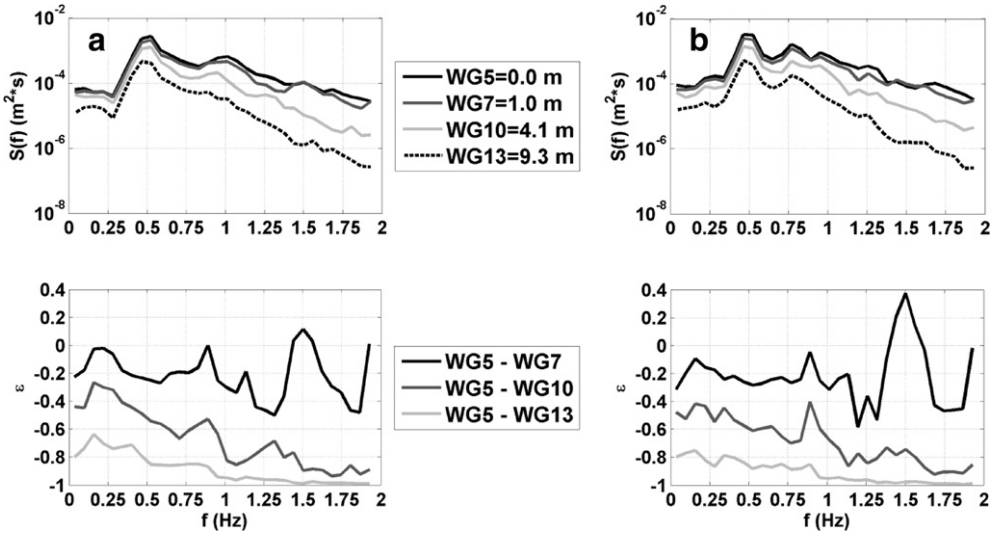

Fig. 7. Band-averaged wave spectral density $S(f)$ (top panes) and normalized energy loss ε (bottom panes) between gauge pairs for (a) single- and (b) double-peaked spectra [(a) $l_s/h = 1.36$, $H_0/h = 0.36$, $h/L_p = 0.09$, $N = 400$ stems/m^2; (b) $l_s/h = 1.36$, $H_0/h = 0.43$, T = 1.25 and 2.0 s, $N = 400$ stems/m^2].

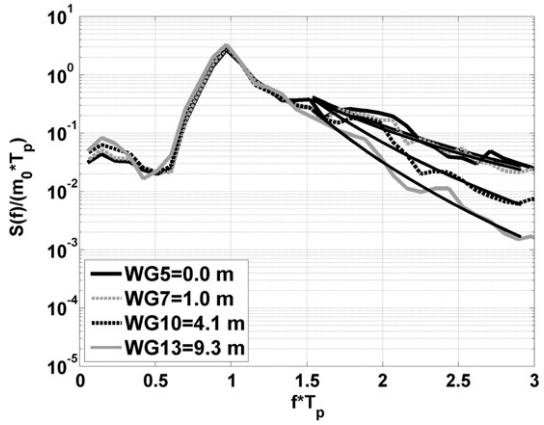

Fig. 8. Evolution of equilibrium range through idealized vegetation for $l_s/h = 1.36$, $H_0/h = 0.36$, $h/L_p = 0.13$, $N = 400$ stems/m^2. The solid line is the fitted f^{-n} parameterization at each location.

be more proportional to an f^{-4} form (Battjes et al., 1987; Toba, 1973; Zakharov and Filonenko, 1967). In order to investigate deviations from the proposed f^{-4} parameterization, single-peaked wave spectra at WG 13 were fitted to the following form:

$$S(f) = af^n \tag{7}$$

where a is a constant and n is the equilibrium range exponent. The equilibrium range was defined as originating at $1.5f_p$ and extending to $3f_p$ (Smith and Vincent, 2003).

The evolution of the spectral tail for one emergent wave condition ($l_s/h = 1.36$, $H_0/h = 0.36$, $h/L_p = 0.13$, $N = 400$ stems/m^2) is shown in Fig. 8, where $S(f)$ is normalized by the zero-moment (m_0) times the peak period. The slope fitted to the equilibrium range steepens with propagation distance through the vegetation field. The values of n at $x = 0$ and 1.0 m closely follow the -4 power law, with values of -4.29 and -4.32, respectively. However, by $x = 4.1$ m, $n = -6.54$. The slope steepens further to -7.86 at $x = 9.3$ m. The dissipation within the equilibrium range was also found to be dependent on submergence ratio and stem density. Table 4 shows the regression results for spectra at WG 13 for the control, $N = 200$ and 400 stems/m^2, where the average n and its standard deviation were calculated for wave conditions grouped by submergence and stem density. The equilibrium range for all spectra, including the control, had an average n value close to the -4 parameterization for the submerged conditions ($l_s/h = 0.78$ and 0.91). However, while the average n for the control spectra continued to follow the -4 power, spectra propagating through emergent vegetation deviate from this value. Furthermore, the spectral tail tends to be more attenuated through denser emergent arrays. The average n values for the control, $N = 200$ and 400 stems/m^2 were -4.11, -5.24 and -6.52, respectively, at $l_s/h = 1.36$. None of the emergent cases were within the f^{-4} parameterization, instead lying within an f^{-5}–f^{-8} range. A steepening of the spectral tail indicates a preferential dissipation of higher frequencies that is independent of the reduction in energy at the spectral peak.

Table 4
Equilibrium range exponents of single-peaked spectra propagating through vegetation (WG 13).

l_s/h	Average n		
	Control	200 stems/m^2	400 stems/m^2
0.78	-4.14 ± 1.37	-3.77 ± 1.48	-3.69 ± 1.59
0.91	-4.52 ± 0.69	-4.43 ± 0.74	-4.56 ± 0.82
1.36	-4.11 ± 0.84	-5.24 ± 0.95	-6.52 ± 1.09

6. Energy dissipation model analysis

Dalrymple et al. (1984) derived the dissipation through vegetation using the conservation of energy flux equation by approximating a vegetation field as an array of rigid, vertical cylinders. Assuming S_v is due only to the drag force F_x, which is expressed as a Morison-type equation, S_v is given by:

$$S_v = \int_{-h}^{-h+l_s} F_x u dz = \int_{-h}^{-h+\alpha h} \frac{1}{2}\rho C_D b N u|u| dz \tag{8}$$

where u is the horizontal velocity of the wave motion. Note that a more correct estimation of F_x is calculated using the relative velocity between the fluid and swaying of the plant stem (Méndez et al., 1999). Evaluating Eq. (8) over the stem length, the energy dissipation for waves propagating through a vegetation field is expressed as:

$$S_v = \frac{2}{3\pi}\rho C_D N d\left(\frac{gk}{\omega}\right)^3 \frac{\sinh^3 k\alpha h + 3\sinh k\alpha h}{3k\cosh^3 kh} A^3 \tag{9}$$

where C_D is the depth-averaged spatial mean bulk drag coefficient, b is the stem diameter, A is the wave amplitude, and $\alpha = l_s/h$ for submerged vegetation and $\alpha = 1$ for emergent vegetation (Dalrymple et al., 1984).

Expanding upon Dalrymple et al. (1984), Méndez and Losada (2004) assumed an unmodified Raleigh distribution and derived wave height evolution for nonbreaking random waves over constant depth as:

$$\frac{H_{rms}}{H_{rms,0}} = \frac{1}{1+\beta x} \tag{10}$$

where,

$$\beta = \frac{1}{3\sqrt{\pi}} C_D N d k \frac{\sinh^3 k\alpha h + 3\sinh k\alpha h}{(\sinh 2kh + 2kh)\sinh kh} H_{rms,0} \tag{11}$$

and H_{rms} is the local wave root-mean-square wave height and $H_{rms,0}$ is the incident root-mean-square wave height. For each of the single-peaked wave conditions, the best fit to the experimental root-mean-square wave height decay was found using a nonlinear least squares method considering C_D as the single calibration variable. Values of C_D ranged from 0.92 to 2.28 with an $R^2 \geq 0.90$ for both $N = 200$ and 400 stems/m^2.

It is useful to define a relationship between C_D and nondimensional flow parameters for predictive purposes where C_D and its associated empirical formulas are specific to *S. alterniflora*. The stem Reynolds number was calculated as:

$$\mathrm{Re} = \frac{u_c b}{\upsilon} \tag{12}$$

where υ is the kinematic viscosity of water (10^{-6} m^2/s) and u_c is the characteristic velocity acting on the plant. The characteristic velocity was defined as the maximum horizontal velocity immediately in the front of the vegetation field (WG 5) at the top of the stems ($z = -h + \alpha h$), with H_{rms} and T_p as the wave height and period corresponding to a monochromatic wave train:

$$u_c = \frac{H_{rms}}{2}\omega_p\left(\frac{\cosh k\alpha h}{\sinh kh}\right) \tag{13}$$

where ω_p is the peak wave angular frequency. The Keulegan–Carpenter number is defined as:

$$\mathrm{KC} = \frac{u_c T_p}{b}. \tag{14}$$

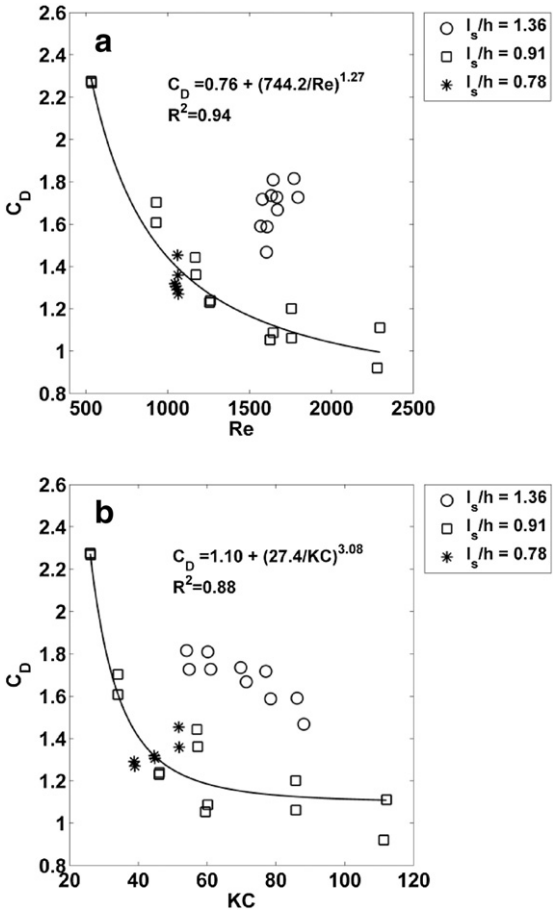

Fig. 9. Bulk drag coefficient C_D as a function of (a) stem Reynolds number Re and (b) Keulegan–Carpenter number KC. The derived equations are fit to submerged conditions ($l_s/h < 1.0$) only. Different symbols represent different values of l_s/h, where $l_s/h = 1.36$ is the circles, $l_s/h = 0.91$ is the squares, and $l_s/h = 0.78$ is the stars.

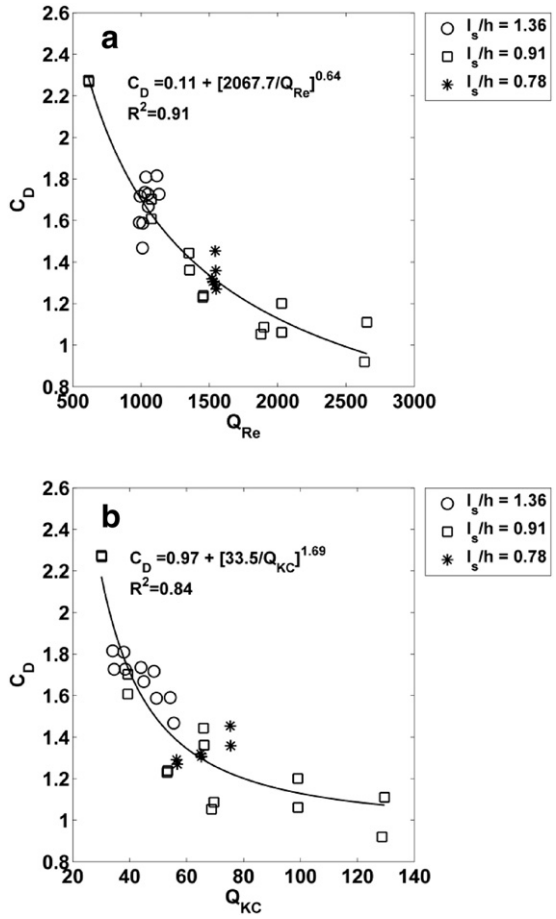

Fig. 10. Bulk drag coefficient C_D as a function of (a) modified stem Reynolds number Q_{Re} and (b) modified Keulegan–Carpenter number Q_{KC} accounting for stem submergence ratio. Different symbols represent different values of l_s/h, where $l_s/h = 1.36$ is the circles, $l_s/h = 0.91$ is the squares, and $l_s/h = 0.78$ is the stars.

To derive the empirical relationship between C_D and the nondimensional numbers Re and KC, the form used by Kobayashi et al. (1993) is fitted:

$$C_D = B + \left(\frac{\kappa}{\mathrm{Re}}\right)^c \text{ and } C_D = B + \left(\frac{\kappa}{\mathrm{KC}}\right)^c. \quad (15)$$

The bulk drag coefficient C_D plotted against Re and KC is shown in Fig. 9 (for 31 cases). Focusing on the submerged vegetation only, C_D decreases with an increasing Re and KC. The fitted values are $(B, \kappa, c) = (0.76, 744.2, 1.27)$ and $(1.10, 27.4, 3.08)$ for $533 < \mathrm{Re} < 2296$ and $26 < \mathrm{KC} < 112$, respectively. The relationship with Re ($R^2 = 0.94$) provides a slightly better fit compared to the one with KC ($R^2 = 0.88$) for the submerged cases.

However, while these coefficients provide a good fit for the modeled submerged conditions, clearly the emergent conditions have much higher C_D values considering the same Re and KC and are not captured by these derived equations. As other studies of submerged vegetation have reported a dependence of C_D on canopy submergence (Méndez and Losada, 2004), C_D as a function of l_s/h was obtained using modified Re and KC parameters defined as $Q_{\mathrm{Re}} = \mathrm{Re}/(l_s/h)^{1.5}$ and $Q_{\mathrm{KC}} = \mathrm{KC}/(l_s/h)^{1.5}$ where the exponent chosen provided the best fit (Fig. 10). Note that l_s/h was capable of being greater than one. The fitted values for Q_{Re} are $(B, \kappa, c) = (0.11, 2067.7, 0.64)$ and for Q_{KC} are $(0.97, 33.5, 1.69)$. Again, the fit is slightly better for Q_{Re} ($R^2 = 0.91$) than Q_{KC} ($R^2 = 0.84$). While Sánchez-González et al. (2011) report a better correlation of C_D with the Keulegan–Carpenter number than with the Reynolds number, this finding is in agreement with Bradley and Houser (2009) who found no improvement in parameterizing C_D with the Keulegan–Carpenter number over the Reynolds number.

The variation of the drag coefficient with stem Reynolds number has most recently been reported by Koftis et al. (2013), Paul and Amos (2011), and Bradley and Houser (2009), among other researchers. However, empirical formulations for *S. alterniflora* are limited as relationships are typically proposed for aquatic plants such as kelp and marine seagrass. Fig. 11 compares the curves of Jadhav (2012) and Wu et al. (2011) for *S. alterniflora* to the proposed equation using the unmodified Reynolds number, with coefficient values shown in Table 5. The proposed equation most closely follows the curve of

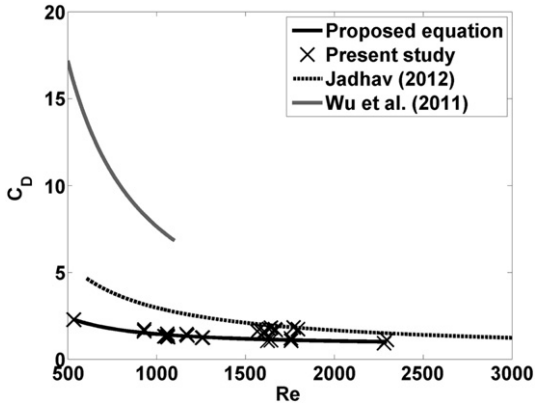

Fig. 11. Variation of bulk drag coefficient C_D with stem Reynolds number Re.

Table 5
Values of coefficients B, κ, c for *S. alterniflora*.

Study	B	κ	c
Jadhav (2012)	0.36	2600	1
Wu et al. (2011)	3.83E−6	5683	1.17
Present study	0.76	744.2	1.27

Jadhav (2012). However, estimated drag coefficients using the proposed equation are smaller at all modeled Reynolds number than the other curves, particularly Wu et al. (2011). One of the reasons for the underestimation by the proposed equation is that both of the comparison studies focused on live *S. alterniflora* and the increased drag induced by the leaves is accounted for in the calibration of C_D. It is difficult to theorize why the curve proposed by Wu et al. (2011) is an order of magnitude higher than the other curves as the study conditions were vastly different. Jadhav (2012) observed submerged *S. alterniflora* under a similar hydrodynamic range to the present study ($600 < \mathrm{Re} < 3200$) during a field campaign; however, Wu et al. (2011) considered very mild wave conditions ($100 < \mathrm{Re} < 1100$) in a laboratory with submergence ratios close to unity. Also, Wu et al. (2011) observed a large scatter in C_D as a function of Re, with $R^2 = 0.43$.

7. Conclusions

Irregular wave spectra were measured over a bed of idealized *S. alterniflora* to study vegetation-induced energy dissipation. The idealized vegetation beds were shown to efficiently attenuate wave energy for single- and double-peaked irregular wave spectra, particularly for emergent conditions. Fitting normalized zero-moment wave heights to an exponential decay model yielded high R^2 values for both spectral types.

A series of single-peaked wave tests were performed, varying submergence, stem density, incident wave height, and peak wave period, in order to determine the importance of these parameters with respect to wave attenuation. Wave attenuation appeared to be most dependent on stem density and submergence as changes in these parameters within the tested range generated the largest response in the decay coefficient k_i. The effect of peak wave period on wave attenuation was inconclusive as conflicting trends were observed in emergent ($l_s/h = 1.36$) and submerged ($l_s/h = 0.78$) regimes, but the range of periods tested was also small. Larger waves were slightly more attenuated through the idealized bed under near-emergent conditions ($l_s/h = 0.91$), although the change in k_i was less than that for submergence. However, the effect of wave height may be coupled to submergence such that wave height is more influential in shallower waters, similar to stem density. Unfortunately, the range of wave conditions was limited to 21 tests, with either wave height or peak period varied at each water level, and the effectiveness of each parameter at multiple submergence ratios was not considered. It is recommended that a wider range of wave parameters be tested to determine the influence of incident wave height and peak period on wave attenuation through coastal vegetation, particular for the transition from the emergent to submerged regime. This transition is of particular importance for coastal salt marshes that are emergent during regular tidal conditions but can become inundated by storm surge.

The attenuation of double-peaked spectra through vegetation was explored by separating the spectra into two wave systems and calibrating k_i for each individual spectrum. These two systems attenuated differently under emergent conditions, where the high-frequency wave system attenuated more than the low-frequency wave system. The difference in attenuation between the two systems increased with denser arrays.

The transformation of single- and double-peaked wave spectra through vegetation was also assessed, with a focus on frequency-dependent attenuation. Energy loss was observed at all frequencies of the spectrum. Although the most obvious loss of energy occurred at the spectral peaks, the energy loss relative to the initial energy increased with higher frequency for both spectral types. This preferential dissipation of higher-frequencies was further investigated by parameterizing the spectral tail as a function of frequency and exploring deviations from the f^{-4} shape. The f^{-4} parameterization did not accurately describe the equilibrium range of irregular single-peaked spectra transforming through emergent vegetation as the spectral tail was found to steepen with propagation distance and denser stem arrays. This evolution of the spectral tail through vegetation is previously undocumented and noteworthy, although for engineering application the effects are likely to be barely noticeable because the energy levels in the tail are small.

A bulk drag coefficient C_D calibrated for submerged *S. alterniflora* decreased with larger stem Reynolds number and Keulegan–Carpenter number, with C_D slightly better correlated with Re. Drag coefficients calibrated for emergent conditions were much greater than those for submerged conditions considering the same Reynolds number, and a modified Re taking into account submergence ratio was required to collapse the data. Most studies have considered only submerged vegetation so this abrupt increase in C_D with Re while transitioning from a submerged to an emergent regime is an active topic of interest. Describing C_D by two curves, one applicable to submerged vegetation and another to emergent, may be more appropriate, but a broad range of Reynolds numbers modeled at submergence ratios ranging from deeply submerged to emergent is required to test this hypothesis. As the range of tested conditions were limited and correspond to a discrete Re and KC range, it is recommended the presented formulations serve as the first estimates of drag coefficients for *S. alterniflora*, with calibration to data serving as the primary methodology.

Acknowledgments

Permission to publish this paper was granted by the Chief of Engineers, US Army Corps of Engineers (USACE). Funding support was provided by the Wave Dissipation by Vegetation for Coastal Protection Work Unit within the USACE Flood and Coastal Systems Program. Duncan B. Bryant, Robert G. W. McComas, Craig J. Fischenich, and William Henderson provided input and support to the laboratory study.

References

Asano, T., Deguchi, H., Kobayashi, N., 1992. Interaction between water waves and vegetation. Proc. 23rd Intern. Coast. Eng. Conf. ASCE, p. 2710-2723.
ASTM Standard D3149, 2006. Standard Specification for Crosslinked Polyolefin Heat-shrinkable Tubing for Electrical Insulation. ASTM International, West Conshohocken, PA (www.astm.org).
ASTM Standard D5323, 2011. Standard Practice for Determination of 2% Secant Modulus for Polyethylene Geomembranes. ASTM International, West Conshohocken, PA (www.astm.org).
Augustin, L.N., Irish, J.L., Lynett, P., 2009. Laboratory and numerical studies of wave damping by emergent and near-emergent wetland vegetation. Coast. Eng. 56, 332–340.
Battjes, J.A., Zitman, T.J., Holthuijsen, L.H., 1987. A re-analysis of the spectra observed in JONSWAP. J. Phys. Oceanogr. 17, 1288–1295.
Bradley, K., Houser, C., 2009. Relative velocity of seagrass blades: implication for wave attenuation in low-energy environments. J. Geophys. Res. 114 (F01004), 1–13.
Callaway, J.C., Josselyn, M.N., 1992. The introduction and spread of smooth cordgrass (*Spartina alterniflora*) in south San Francisco Bay. Estuaries 15, 218–226.
Camfield, F.E., 1977. A Method for Estimating Wind-wave Growth and Decay in Shallow Water With High Values of Bottom Friction. CETA 77-6 Coastal Engineer Research Center, Fort Belvoir, VA.
Cavallaro, L., Re, C.L., Paratore, G., Viviano, A., Foti, E., 2010. Response of *Posidonia oceanica* to wave motion in shallow-waters — preliminary experimental results. Proc. 32nd Intern. Coastal Eng. Conf., Coas. Eng. Res. Council, pp. 1–10.
Chatagnier, J., 2012. The Biomechanics of Salt Marsh Vegetation Applied to Wave and Surge Attenuation. (Master of Science) Louisiana State University (64 pp.).
Chen, Q., Zhao, H., 2012. Theoretical models for wave energy dissipation cause by vegetation. J. Eng. Mech. 138, 221–229.

Cooper, N.J., 2005. Wave dissipation across intertidal surfaces in the Wash Tidal Inlet, Eastern England. J. Coast. Res. 21, 28–40.

Dalrymple, R.A., Kirby, J.T., Hwang, P.A., 1984. Wave diffraction due to areas of energy dissipation. J. Waterw. Port Coast. Ocean Eng. 110, 67–79.

Dubi, A., Tørum, A., 1996. Wave energy dissipation in kelp vegetation. Proc. 25th Intern. Coast. Eng. Conf. ASCE, pp. 2626–2639.

Feagin, R.A., Mukherjee, N., Shanker, K., Baird, A.H., Cinner, J., Kerr, A.M., Koedam, N., Sridhar, A., Arthur, R., Jayatissa, L.P., Lo Seen, D., Menon, M., Rodriguez, S., Shamsuddoha, M., Dahdouh-Guebas, F., 2009. Conserv. Lett. 3, 1–11.

Feagin, R.A., Irish, J.L., Möller, I., Williams, A.M., Colón-Rivera, R.J., Mousavi, M.E., 2011. Short communication: engineering properties of wetland plants with application to wave attenuation. Coast. Eng. 58, 251–255.

Fonseca, M.S., Cahalan, J.A., 1992. A preliminary evaluation of wave attenuation by four species of seagrass. Estuar. Coast. Shelf Sci. 35, 565–576.

Freeman, G.E., Rahmeyer, W.J., Copeland, R.R., 2000. Determination of Resistance Due to Shrubs and Woody Vegetation. ERDC/CHL TR-00-25 U.S. Army Engineer Research and Development Center, Vicksburg, MS.

Goda, Y., Suzuki, Y., 1976. Estimation of incident and reflected waves in random wave experiments. Proc. 15th Intern. Coast. Eng. Conf. ASCE, pp. 828–845.

Jadhav, R.S., 2012. Field Investigation of Wave and Surge Attenuation in Salt Marsh Vegetation and Wave Climate in a Shallow Estuary. (Doctor of Philosophy) Louisiana State University (120 pp.).

Jadhav, R.S., Chen, Q., Smith, J.M., 2013. Spectral distribution of wave energy dissipation by salt marsh vegetation. Coast. Eng. 77, 99–107.

Knutson, P.L., Brochu, R.A., Seelig, W.N., Inskeep, M., 1982. Wave damping in *Spartina alterniflora* marshes. Wetlands 2, 87–104.

Kobayashi, N., Raichle, A.W., Asano, T., 1993. Wave attenuation by vegetation. J. Waterw. Port Coastal Ocean Eng. 119, 30–48.

Koch, E.W., Sanford, L.P., Chen, S.N., Shafer, D.J., Smith, J.M., 2006. Waves in Seagrass Systems: Review and Technical Recommendations. ERDC TR-06-15 U.S. Army Engineer Research and Development Center, Vicksburg MS.

Koftis, T., Prinos, P., Stratigaki, V., 2013. Wave damping over artificial *Posidonia oceanica* meadow: a large-scale experiment study. Coast. Eng. 73, 71–83.

Krauss, K.W., Doyle, T.W., Doyle, T.J., Swarzenski, C.M., From, A.S., Day, R.H., Conner, W.H., 2009. Water level observations in mangrove swamps during two hurricanes in Florida. Wetlands 29, 142–149.

Leonard, L.A., Luther, M.E., 1995. Flow hydrodynamics in tidal marsh canopies. Limnol. Oceanogr. 40, 1474–1484.

Lima, S.F., Neves, C.F., Rosauro, N.M.L., 2006. Damping of gravity waves by fields of flexible vegetation. Proc. 30th Intern. Coast. Eng. Conf, pp. 491–503.

Løvås, S.M., Tørum, A., 2000. Effect of the submerged vegetation upon wave damping and run-up on beaches: a case study of *Laminaria hyperborea*. Proc. 27th Intern. Coast. Eng. Conf. ASCE, pp. 851–864.

Lowe, R.J., Falter, J.L., Koseff, J.R., Monismith, S.G., Atkinson, M.J., 2007. Spectral wave flow attenuation within submerged canopies: implications for wave energy dissipation. J. Geophys. Res. 112 (C05018), 1–14.

Manca, E., Cáceres, I., Alsina, J., Stratigaki, V., Townend, I., Amos, C.L., 2012. Wave energy and wave-induced flow reduction by full-scale model *Posidonia oceanica* seagrass. Cont. Shelf Res. 50–51, 110–116.

Mazda, Y., Magi, M., Ikeda, Y., Kurokawa, T., Asano, T., 2006. Wave reduction in a mangrove forest dominated by *Sonneratia* sp. Wetlands Ecol. Manag. 14, 365–378.

Mei, C.C., Chan, I., Liu, P., Huang, Z., Zhang, W., 2011. Long waves through emergent vegetation. J. Fluid Mech. 687, 461–491.

Méndez, F.J., Losada, I.J., 2004. An empirical model to estimate the propagation of random breaking and nonbreaking waves over vegetation fields. Coast. Eng. 51, 103–118.

Méndez, F.J., Losada, I.J., Losada, M.A., 1999. Hydrodynamics induced by wind waves in a vegetation field. J. Geophys. Res. 104, 18383–18396.

Möller, I., 2006. Quantifying saltmarsh vegetation and its effect on wave height dissipation: results from a UK East coast saltmarsh. Estuarine Coastal Shelf Sci. 69, 337–351.

Möller, I., Spencer, T., 2002. Wave dissipation over macro-tidal saltmarshes: effects of marsh edge typology and vegetation change. J. Coast. Res. S136, 506–521.

Möller, I., Spencer, T., French, J.R., Leggett, D.J., Dixon, M., 1999. Wave transformation over salt marshes: a field and numerical modeling study from North Norfolk, England. Estuar. Coast. Shelf Sci. 49, 411–426.

Mork, M., 1996. The effect of kelp in wave damping. Sarsia 80, 323–327.

Mullarney, J.C., Henderson, S.M., 2010. Wave-forced motion of submerged single-stem vegetation. J. Geophys. Res. 115 (C12061), 1–14.

Nepf, H.M., 2012. Flow and transport in regions with aquatic vegetation. Ann. Rev. Fluid Mech. 44, 123–142.

Neumeier, U., Ciavola, P., 2004. Flow resistance and associated sedimentary processes in a *Spartina maritima* salt-marsh. J. Coast. Res. 20, 435–447.

Paul, M., Amos, C.L., 2011. Spatial and seasonal variation in wave attenuation over *Zostera noltii*. J. Geophys. Res. 116 (C08019), 1–16.

Pezeshki, S.R., Choi, H.S., DeLaune, R.D., 1993. Population differentiation in *Spartina patens*: water potential components and bulk modulus of elasticity. Biol. Plant. 35, 43–51.

Phillips, O.M., 1958. The equilibrium range in the spectrum of wind-generated waves. J. Fluid Mech. 4, 426–434.

Quartel, S., Kroon, A., Augustinus, P.G.E.F., Van Santen, P., Tri, N.H., 2007. Wave attenuation in coastal mangroves of the Red River Delta, Vietnam. J. Asian Earth Sci. 29, 576–584.

Resio, D.T., Long, C.E., Vincent, C.L., 2004. Equilibrium-range constant in wind-generated wave spectra. J. Geophys. Res. 109 (C01018), 1–14.

Salpeter, K.E., Millemann, D.R., Caputo, M.F., White, B.L., Touchette, B.W., 2012. Delayed modifications in plant-water relations in the coastal marsh halophyte *Spartina patens* following sudden increases in soil salinity. Bot. Mar. 55, 307–310.

Sánchez-González, J.F., Sánchez-Rojas, V., Memos, C.D., 2011. Wave attenuation due to *Posidonia oceanica* meadows. J. Hydraul. Res. 49, 503–514.

Smith, J.M., 2007. Full-plane STWAVE with Bottom Friction: II. Model Overview. ERDC TN-SWWRP-07-5 U.S. Army Engineer Research and Development Center, Vicksburg, MS.

Smith, J.M., Vincent, C.L., 2003. Equilibrium ranges in surf zone wave spectra. J. Geophys. Res. 108 (3366), 1–11.

Smith, J.M., Jensen, R.E., Kennedy, A.B., Dietrich, J.C., Westerink, J.J., 2010. Waves in wetlands: hurricane Gustav. Proc. 32nd Intern. Coast. Eng. Conf. ASCE, pp. 1–12.

Stratigaki, V., Manca, E., Prinos, P., Losada, I.J., Lara, J.L., Sclavo, M., Amos, C.L., Cáceres, I., Sánchez-Arcilla, A., 2011. Large-scale experiments on wave propagation over *Posidonia oceanica*. J. Hydraul. Res. 49, 31–43.

Toba, Y., 1973. Local balance in the air-sea boundary processes on the spectrum of wind waves. J. Oceanogr. Soc. Jpn 29, 209–220.

Touchette, B.W., Rhodes, K.L., Smith, G.A., Poole, M., 2009. Salt spray induces osmotic adjustment and tissue rigidity in smooth cordgrass, *Spartina alterniflora* (Loisel.). Estuar. Coast. 32, 917–925.

Tschirky, P., Hall, K., Turcke, D., 2000. Wave attenuation by emergent wetland vegetation. Proc. 27th Intern. Coast. Eng. Conf. ASCE, pp. 865–877.

USDA, NRCS, 2012. The PLANTS Database. National Plant Data Team, Greensboro, NC (http://plants.usda.gov).

Vo-Luong, P., Massel, S.R., 2008. Energy dissipation in non-uniform mangrove forests of arbitrary depth. J. Mar. Syst. 74, 603–622.

Wayne, C.J., 1976. The effect of sea and marsh grass on wave energy. Coast. Res. Notes 4, 6–8.

Wu, W., Ozeren, Y., Wren, D.I., Chen, Q., Zhang, G., Holland, M., Ding, Y., Kuiry, S.N., Zhang, M., Jadhav, R., Chatagnier, J., Chen, Y., Gordji, L., 2011. SERRI project: investigation of surge and wave reduction by vegetation. SERRI Report 80037-01. National Center for Computational Hydroscience and Engineering, University of Mississippi.

Ysebaert, T., Yang, S.L., Zhang, L., He, Q., Bouma, T.J., Herman, P.M.J., 2011. Wave attenuation by two contrasting ecosystem engineering salt marsh macrophytes in the intertidal pioneer zone. Wetlands 31, 1043–1054.

Zakharov, V.E., Filonenko, N.N., 1967. Energy spectrum for stochastic oscillations on the surface of a liquid. Sov. Phys. Dokl. 11, 881–883.